Materials and Design 188 (2020) 108424

Contents lists available at ScienceDirect

Materials and Design

journal homepage: www.elsevier.com/locate/matdes

A novel auxetic structure based bone screw design: Tensile mechanical characterization and pullout fixation strength evaluation

Yan Yao [a,b,c], Lizhen Wang [a,b,*], Jian Li [b,d], Shan Tian [a,b], Ming Zhang [c], Yubo Fan [a,b,d,**]

[a] Key Laboratory for Biomechanics and Mechanobiology of Ministry of Education, School of Biological Science and Medical Engineering, Beihang University, Beijing 100083, China
[b] Beijing Advanced Innovation Center for Biomedical Engineering, Beihang University, Beijing 100083, China
[c] Department of Biomedical Engineering, Faculty of Engineering, The Hong Kong Polytechnic University, Hong Kong, China
[d] Beijing Key Laboratory of Rehabilitation Technical Aids for Old-Age and Disability, Key Laboratory of Rehabilitation Aids Technology and System of the Ministry of Civil Affairs, National Research Center for Rehabilitation Technical Aids, Beijing 100176, China

HIGHLIGHTS

- Auxetic bone screws were designed and explored for the first time.
- The designed screw can be fabricated by SLM 3D-printing method.
- Varying auxetic structures altered the screw's mechanical properties especially its functional properties.
- The bone-screw fixation could be improved by auxetic structures while it is also affected by other design factors.

GRAPHICAL ABSTRACT

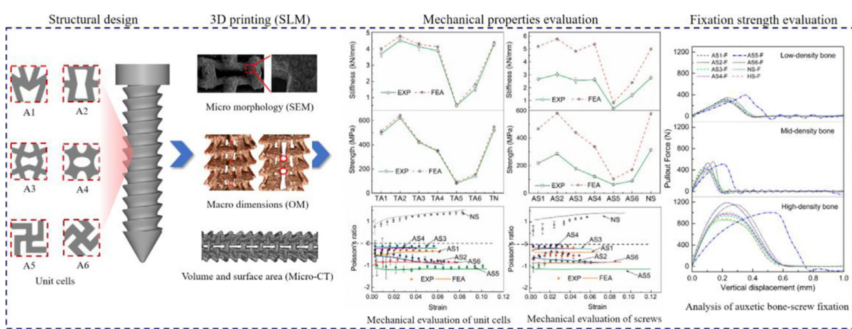

ARTICLE INFO

Article history:
Received 9 October 2019
Received in revised form 3 December 2019
Accepted 12 December 2019
Available online 17 December 2019

Keywords:
Bone screw
Auxetic structure
3D printing
Mechanical properties
Pullout force

ABSTRACT

It was supposed that auxetic structure with negative Poisson's ratio (NPR) expands under stretch and could enhance the screw-bone fixation. In this study, the novel auxetic structure based bone screws were designed, and mechanical properties and fixation strength were evaluated. Auxetic unit cells (A1–A6) were introduced into the design of screw bodies after a mechanical evaluation. Tubular auxetic structures (TA1–TA6), auxetic screws (AS1–AS6) and one non-auxetic screw (NS) were manufactured using 3D-printing. The fabrication process well reproduced the original designs despite the some mismatch in the macro and micro morphologies. Tensile tests on specimens were conducted experimentally and computationally. The relationship between NPR and fixation strength of the screws was investigated by computationally bone-pullout test. Among all screw designs, AS2 generated the largest stiffness and strength, and better NPR, AS5 produced the highest NPR, and smallest stiffness and strength. Maximal pullout force within low-, mid- and high-density bone was shown in AS5 (399.39 N), AS6 (561.07 N) and AS2 (1185.93 N) respectively. It was concluded that varying auxetic structures altered the screw's mechanical properties especially its functional properties. The bone-screw fixation could be improved by auxetic structures while other design factors should also be taken in account.

* Correspondence to: L. Wang, Key Laboratory for Biomechanics and Mechanobiology of Ministry of Education, School of Biological Science and Medical Engineering, Beihang University, Beijing 100083, China.
** Correspondence to: Y. Fan, Beijing Key Laboratory of Rehabilitation Technical Aids for Old-Age and Disability, Key Laboratory of Rehabilitation Aids Technology and System of the Ministry of Civil Affairs, National Research Center for Rehabilitation Technical Aids, Beijing 100176, China.
E-mail addresses: lizhenwang@buaa.edu.cn (L. Wang), yubofan@buaa.edu.cn (Y. Fan).

https://doi.org/10.1016/j.matdes.2019.108424

1. Introduction

Bone screws are widely used in orthopedics for fracture fixation [1], while more than 10% of fixation failure was associated with screw migration and after-implant pull-out due to weak bone-screw fixation [2–5]. Bone cement was usually used to enhance the fixation strength of screw in clinic, but many complications occurred usually [2,3]. The fixation strength of bone screw could be improved by proper structural designing without using cement. It was proposed that the fixation strength of the screw could be improved by increasing its contact area to the bone and optimizing the fixation mechanism in the interface (e.g. enlarging the diameter and length of the screw or introducing the push-fit structure based on barbed fixation mechanism) [4–6]. However, these approaches were found to risk fixation success by causing damage and absorption to the surrounding bone tissue. A novice solution to the challenging problem is not yet clear.

Auxetic structure with a negative Poisson's ratio (NPR) would expand in the transverse direction under stretch (or shrink under contraction) [7] and thus possess the unprecedented advantage in special application [8–13]. Bone screw with NPR property could enhance the bone-screw fixation strength by expanding to resist pulling and resuming deformation when unloaded to avoid causing additional damage. However, the design of auxetic bone screw was rarely investigated. The Poisson's ratio of object could be adjusted from positive to negative by auxetic structural designing [14,15]. Previously, Ren's group designed and evaluated the first auxetic nail, though nails with auxetic structure were supposed to exert easier push-in and harder pull-out, findings in their study were less consistent upon repeating tests [16]. We speculated that the design of the auxetic structure was preliminary to produce more conclusive outcomes. Other studies showed that it's difficult to balance the strength, stiffness and NPR property in the process of auxetic structure designing [17,18]. A proper design is necessary for special application.

In this study, it was hypothesized that the fixation strength of bone screw could be increased by introducing the auxetic unit cells to the design of bone screw (through radially expanding under longitudinal pull-out load). As the strength & stiffness and NPR of structure are highly determined by the geometrical shape of the auxetic structure, it is necessary to explore more kinds of auxetic structural design for superior performance. Besides, the porosity and pore size of auxetic structure should be carefully designed to promote fluid transportation and improve the osseointegration as a porous implant used in bone [19,20].

Different designs of the auxetic structures had been studied in literature [17,21–28]. However, most of the works were confined to two-dimension (2D) due to the limitations of the manufacturing process. Three-dimensional (3D) printing technique enables the fabrication of complex structures both conveniently and accurately based on CAD models [29–31]. The technology provides possibility for the design, fabrication and mechanical evaluation of auxetic bone screws with varying designs.

In this study, six kinds of auxetic unit cells were introduced into the design of bone screw and one typical non-auxetic unit was used as comparison. The tensile stiffness & strength and Poisson's ratio of designed unit cells and screws were evaluated by tensile test and finite element analysis (FEA). The pullout fixation strength of auxetic bone screws (ASs), non-auxetic bone screw (NS) and hollow bone screw (HS, used in clinic) were compared based on FEA. These preliminary investigations would give guidance to the design of anti-pullout bone screw, which might provide new insights into solving the loosening and pulling out problem of bone screw.

2. Design and fabrication

2.1. Design of auxetic unit cells and auxetic bone screws

Auxetic structures were classified into three types including re-entrant structures, chiral structures and rotating structures [32] according to geometrical shape and deformation mechanism of the unit cells. Based on this, six kinds of auxetic unit cells (Fig. 1b A1–A6) were designed and used in the study. One non-auxetic unit (N) was set as the control (Fig. 1b N). The designed unit cells were planer 3 mm × 3 mm, with pore sizes of 358–1260 μm, in consideration of the ideal pore size for bone tissue engineering (300–1200 μm [33–35]) and the precision of 3D printing. The porosity was set 0.53 and kept consistent across all designed unit cells, ensuring the good osseointegration of the designed bone screw [36–38].

The designed bone screw was shown in Fig. 1a, with reference of the Standard Specification for Metallic Medical Bone Screws (Designation: F 543–07). Models of tubular auxetic\non-auxetic structures (TA\TN, with a hollow central column, and t is the wall thickness) and screw bodies were developed using Pro/E (Wildfire 5.0, PTC, USA) (Fig. 1c and d). Here noted that the anisotropic unit cells (A1 and A2) were used in following study because they have better mechanical properties in Y direction than X direction based on the FEA results (Supplementary material Fig. 1).

2.2. Materials and fabrication process

Selected laser melting (SLM) 3D printing is a powder bed fusion based additive manufacturing process, which was used for the fabrication of designed bone screws. SLM specimens were manufactured using the parametric setups of 100 μm laser beam spot, 200 °C preheat temperature, and 50 μm powder thickness (FS121M, Farsoon, China) (Fig. 2b). Ti6Al4V powders were selected as the printing materials with mean particle size of 50 μm (Arcam AB, Gothenburg, Sweden) and density of 4.5 g/cm^3 (Fig. 2c). The printing direction is parallel to the layer direction in SLM processes. After printed, the specimens were washed by isopropyl alcohol for several times and then sunk in distilled water for half an hour in an ultrasonic cleaner to remove the unsintered powder. Three specimens were fabricated for each of designed tubular structures (t = 0.8 mm) and screws (t = 1.2 mm).

3. Experiments

3.1. Morphological characterization

The macro dimensions of the fabricated specimens were analyzed using the optical microscope (OM). Twenty strut thicknesses and pore sizes in random location were obtained and their average dimensions were calculated (Fig. 2e). The micro morphology was analyzed using the Scanning Electron Microscope (SEM) (Qoanta 250, FEI, USA), with the voltage of 5.0 kV and the magnification of ×100–×500 (Fig. 2d). Micro-CT (SkyScan1176, Bruker, Belgium) was used to measure the volume and surface area of specimen with the tube voltage of 90 kV, tube current of 180 μA, and resolution of 17 μm (Fig. 2f).

3.2. Tensile testing

Poisson's ratio was defined as the ratio of the transverse contraction strain to the longitudinal extension strain in the direction of stretching force as:

$$v = -\varepsilon_x/\varepsilon_y \tag{1}$$

where v is Poisson's ratio, ε_x and ε_y are the transverse contraction strain and longitudinal extension strain. In this study, the Poisson's ratio, stiffness and strength were tested using standard quasi-static uniaxial tensile experiment at the speed of 1 mm/min using 10 kN Instron Machine (AG-IS, SHMADZU, Japan) according to the ISO standard (references here). The stress-strain curve was obtained for each specimen. Points on the outer diameter in the middle of the screw body were marked in order to calculate the Poisson's ratio during the tensile deformation (Fig. 2g). The positions of these points were recorded using a

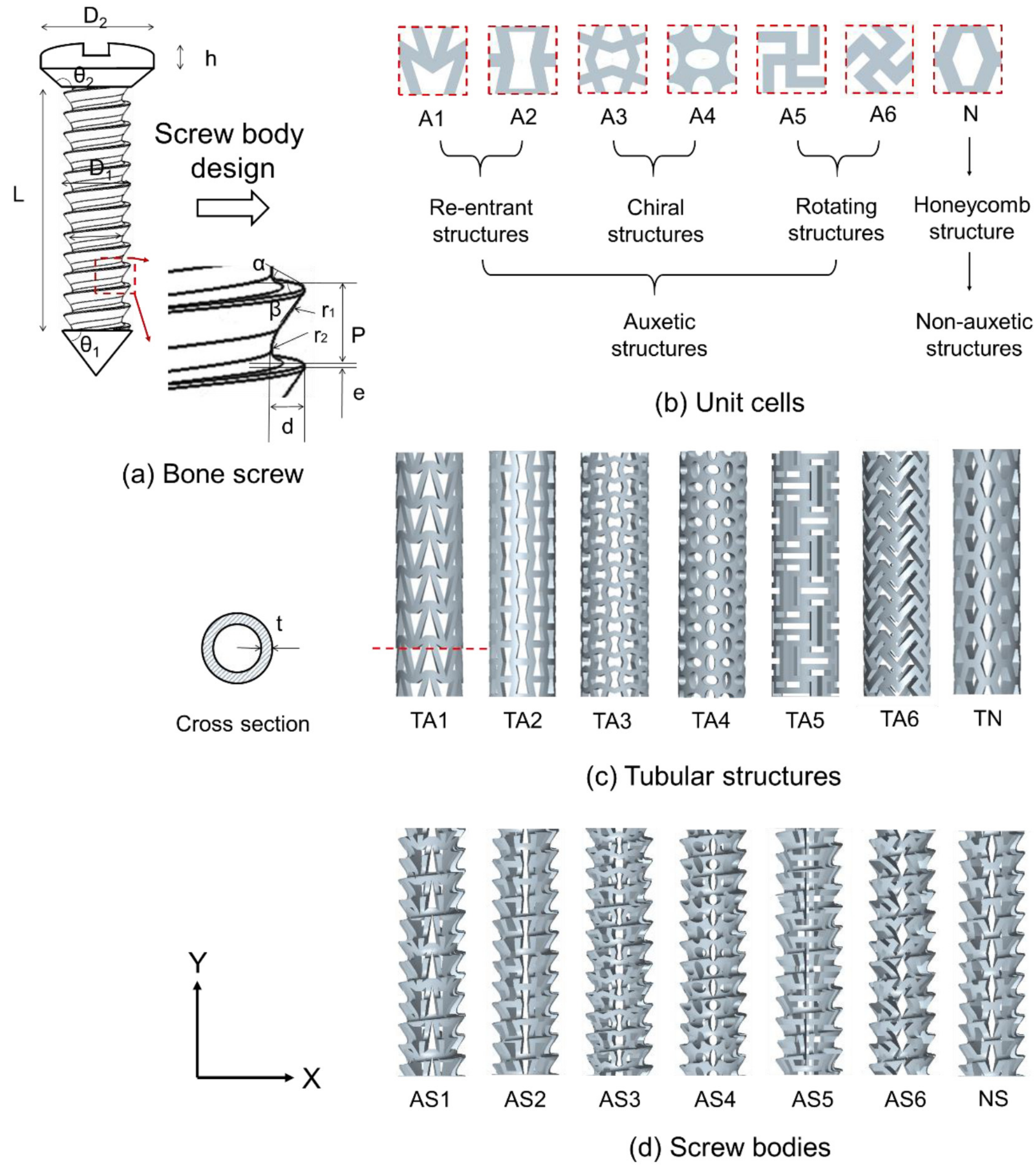

Fig. 1. Schematic diagram of the designed screws. (a) Geometrical configurations of the designed bone screw (D_1 = 5.7 mm, L = 21 mm, t = 0.8 mm, P = 1.75 mm, d = 0.75 mm, e = 0.1 mm, α = 35°, β = 87°, r_1 = 1, r_2 = 0.3); (b) Auxetic unit cells (A1–A6) and non-auxetic unit cell (N); (c) Designed tubular structures: TA1, TA2, TA3, TA4, TA5, TA6, and TN; (d) Designed screw bodies: AS1, AS2, AS3, AS4, AS5, AS6, and NS.

stereomicroscope (K-400L, Motic, China), with a photographing frequency of 2 Hz and a magnification of ×7.5. The images were post-proceeded in the image analysis software (I-SPEED 3 Suite software, Olympus, Japan), which quantified the displacements of the pre-marked points (Fig. 2g). Facilities for the uniaxial tension test were shown in Fig. 2g. All three specimens of each type were tested to generate the averaged results.

3.3. Finite element analysis

The tensile mechanical performance of the designed tubular structures (t = 0.8, 1.2, 1.6 mm, outer diameter D_1 was maintained) and screws (t = 1.6 mm) were investigated using FEA. The uniaxial Poisson's ratio, tensile stiffness, and strength of the screws were reported by Abaqus Explicit solver (6.14, SIMULIA Inc., USA). The model was discretized of 844183 tetrahedral (C3D4) elements with an average size of 0.1 mm, and there are totally 207148 nodes (taking AS1 for example). Material properties of the screws were shown in Fig. 3 and Table 1. The tubular structures and screws were modelled as a homogeneous elasto-plastic material with Drucker-Prager representation. Ductile failure with damage evolution was used as the failure criterion. All the degrees of freedom of the bottom surface nodes. Nodes on the top surface were constrained to only move along the longitudinal direction. Displacement was defined during the simulation according to the experimental test condition. The trajectories of the points on the middle of screw body were recorded to calculate the Poisson's ratio (Fig. 2h).

In order to investigate the relationship between auxetic performance and the fixation strength of the designed bone screws, Abaqus Explicit solver (6.14, SIMULIA Inc., USA) was used to simulate the pull-out processes. It was assumed that bone tissue had fully grown into the thread of screw (but had not grown into the porous of screw, which aims to avoid the effect of bone ingrowth). The bone was simplified as a 27 × 27 × 36 mm rectangle and meshed with 250804 C3D4 elements, and the region close to the screw-bone interface was meshed with finer elements of 0.2 mm using Hypermesh (13.0, Altair Engineering Corp, USA). The screw was meshed by C3D4 elements with an

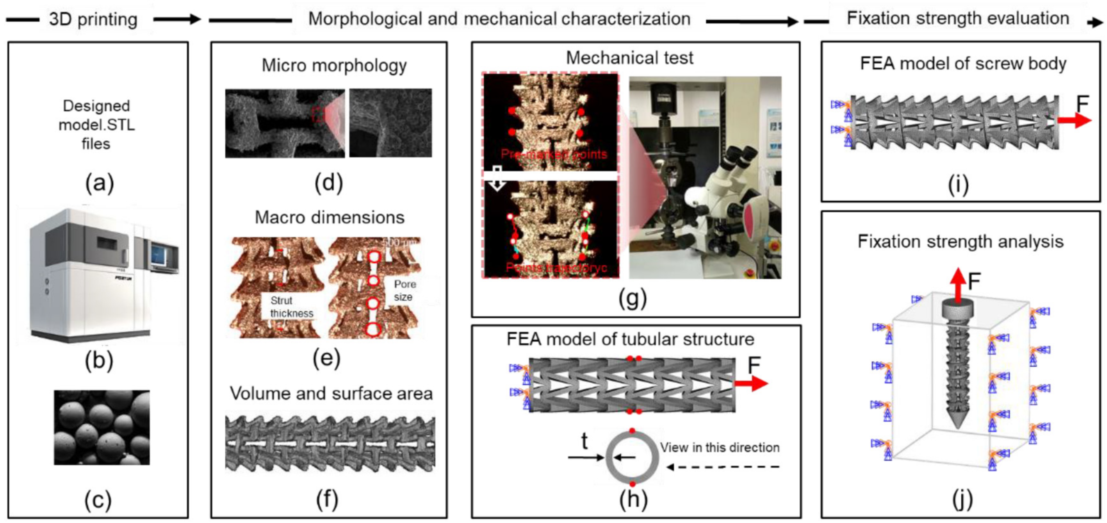

Fig. 2. (a) STL files of screw models; (b) Selected laser melting (SLM) 3D Printer; (c) Ti-6Al-4V Powder; (d) Micro morphology analysis (used by SEM); (e) Strut thickness and Pore size measurement (used by OM); (f) Volume and surface area measurement (used by Micro-CT); (g) Mechanical test under uniaxial tension (points marked with red color were used to record the deformation of the structure); (h) FEA model of the tubular structure; (i) FEA model of the screw body; (j) Pullout process simulation of bone screw.

average size of 0.2 mm. Material properties of the bone and screws were shown in Fig. 3 and Table 1. In this study, three kinds of cancellous bones were chosen to investigate the effect of bone density on the anti-pullout performance of auxetic bone screw, the cortical bone was not considered because of the small contact area with the screw. The bone was modelled as a homogeneous elasto-plastic material with Drucker-Prager representation [39]. Ductile failure with damage evolution was used as the failure criterion. Hard surface-to-surface contact was assigned to the screw-bone interface, with a coefficient of friction of 0.61 [40]. All the external surface of bone was fixed except for nodes at the top and bottom surfaces. An average displacement velocity of 15 mm/s was applied to the screw head along the longitude axis.

4. Result

4.1. Morphological characterization

It was shown that the surface of printed specimen is roughened due to the adhering spherical particles. The shape of the printed struts and pores were well reproduced, but excessive material was found in the corner of different pores (Fig. 4), especially in fabricated screws. In addition, a strut surface also displayed in Fig. 4. No inter-layer differentiation was shown on specimens of hollow cylindrical structures and screws,

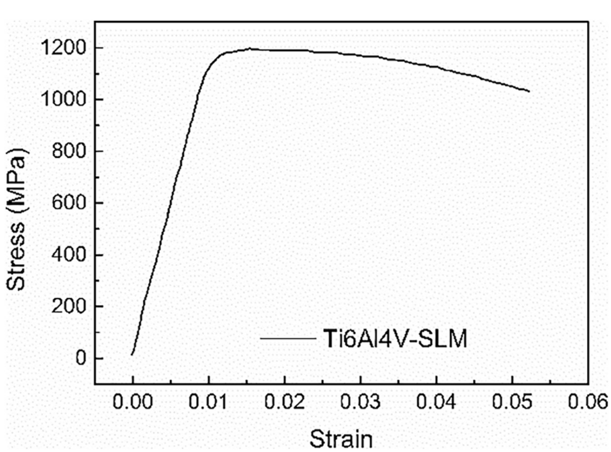

Fig. 3. Stress-strain curve of Ti6Al4V-SLM obtained by uniaxial testing.

which indicated the complete melting of metal powder and metallurgical bonding between layers in SLM fabrication process.

The average strut, pore size, volume and surface area of the specimens were illustrated in Fig. 5a and b, respectively. It was found that the printed tubular structures were slightly different in pore and strut size, volume, and surface area compared to the original designs. While, for the screws this mismatch was significant. The accuracy of SLM manufacturing was affected by the pore shape. Relative errors for pore and strut size, volume, and surface area were shown in Supplementary Material (Tables 1 and 2).

4.2. Mechanical properties

4.2.1. Mechanical properties of designed unit cells

Results of the tensile experiment (EXP) and FEA for the designed tubular structures ($t = 0.8$ mm) were illustrated in Fig. 6a, b. In the tensile tests, TA2 exhibited the largest tensile stiffness (4.54 ± 0.13 kN/mm) and strength (621.56 ± 4.99 MPa) among all the screws, while TA5 exhibited the smallest tensile stiffness (0.50 ± 0.06 kN/mm) and strength (81.77 ± 0.43 MPa). The detailed value results were shown in Supplementary Material (Table 3). A good agreement was shown in tensile stiffness and strength between the experiments and simulations. There was a trend that both of the two mechanical attributes increased as the wall thickening (0.8 to 1.6 mm) (Fig. 6c and d). The detailed value results were shown in Supplementary Material (Table 5). Predictably, TN produced a positive Poisson's ratio while those of all the TAs were negative. Tensile strain was found influence the magnitude of Poisson's ratio. Maximum NPR was -0.54 ± 0.28, -0.83 ± 0.06, -0.13 ± 0.06, -0.29 ± 0.15, -1.20 ± 0.08 and -0.96 ± 0.19 for TA1 to TA6 respectively in the process of tensile deformation (Fig. 6e). Wall thickness could increase the breaking elongation rate but had limited effects on the Poisson's ratio (Fig. 6f).

Table 1
Material properties of bone and Ti6Al4V.

	Bone [41–43]			Ti6Al4V-SLM
Young's modulus (MPa)	48.75	200	400	120
Poisson's ratio	0.25	0.25	0.35	0.3
Density (10^{-4} g/mm^3)	2	2.6	3.5	45.1
Fracture strain (%)	4	2.3	10	4
Yield stress (MPa)	1.95	2.5	4	1124

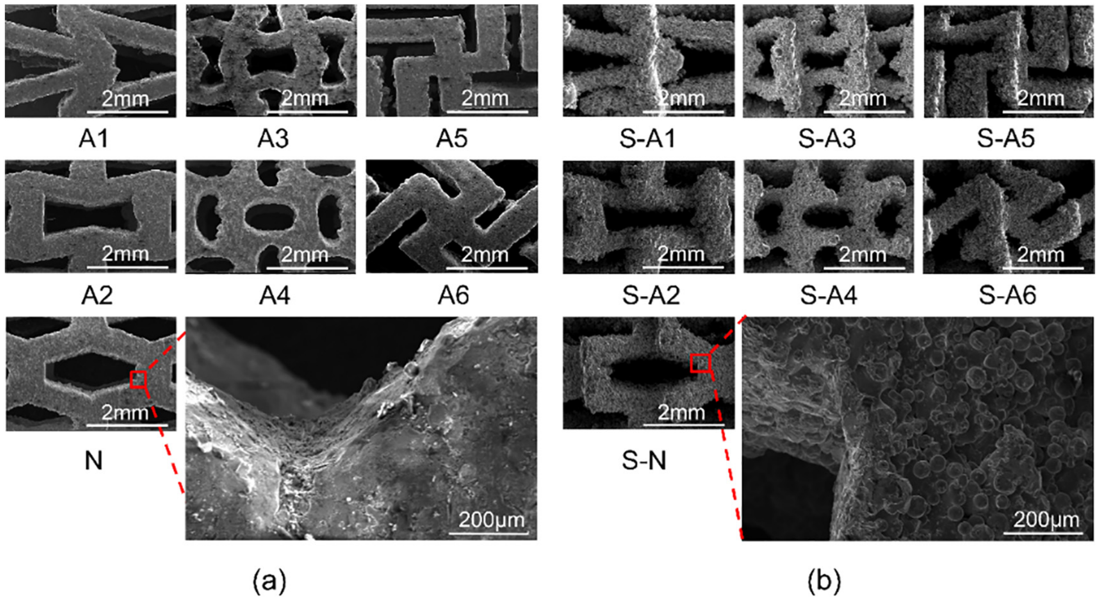

Fig. 4. SEM images of pore morphology and micro structural surface characteristics. (a) Unit cells of the fabricated tubular structures (A1, A2, A3, A4, A5, A6, and N); (b) Unit cells of the fabricated screw bodies (S-A1, S-A2, S-A3, S-A4, S-A5, S-A6, and S—N).

4.2.2. Mechanical properties of designed bone screws

Results of EXP and FEA for the designed screws (t = 1.6 mm) were illustrated in Fig. 7. A good agreement was found between the experiments and simulations for the mechanical evaluation of different auxetic screws, in spite that values in tensile stiffness, strength, and Poisson's ratio were different, while this different was acceptable as described in previous studies [47–49]. AS2 exhibited the largest tensile stiffness (EXP: 3.04 $\pm$ 0.19 kN/mm, FEA: 5.78 kN/mm) and strength (EXP: 286.87 $\pm$ 8.62 MPa, FEA: 578.66 MPa) among all the screws. AS5 exhibited the smallest tensile stiffness (EXP: 0.39 $\pm$ 0.04 kN/mm, FEA: 0.86 kN/mm) and strength (EXP: 63.08 $\pm$ 4.31 MPa, FEA: 102.90 MPa) (Fig. 7a and b). The detailed value results were shown in Supplementary Material (Tables 4 and 5). NS produced a positive Poisson's ratio while those of all the ASs were negative. Maximum NPR was EXP: -0.28 ± 0.001, -0.66 ± 0.13, -0.15 ± 0.07, -0.16 ± 0.03, -1.09 ± 0.21 and $-0.69 \pm 0.0.06$, FEA: -0.38, -0.83, -0.22, -0.24, -1.14 and -0.86 for AS1 to AS6 respectively under tensile loading (Fig. 7c). Besides, cutting thread decreased the tensile stiffness & strength and breaking elongation, while had almost no effect on auxetic behavior compared screws (t = 1.6 mm) to tubular structures (t = 1.6 mm).

4.3. Pullout force

The pullout force vs. pullout vertical displacement (PVD) plots (Fig. 8) demonstrated a similar trend across all tested screws—as displacement progressed, the pullout force gradually increased until reaching its peak midway due to the broken bone tissues. The pullout force then declined to zero and evened out as displacement continued. In regardless of screw types, the average magnitude of pullout forces was positively proportional to bone density. AS1–AS6 had higher pullout forces than NS and HS in all three bone-density groups. The maximum pullout in low-, mid- and high-density bones were shown in AS5 (399.39 N), AS6 (561.07 N) and AS2 (1185.93 N) respectively. The detailed value results were shown in Supplementary Material (Table 6). It was also found that PVD of bone screw was affected by the bone fracture strain, the larger the strain was, and the greater the PVD was. Besides, different screws had different fracture PVDs, AS5 had the largest fracture PVD among all three bones.

5. Discussion

Bone screw composed of auxetic unit cells was supposed to enhance the bone-screw fixation. Moreover, bone screws composed of auxetic structure would show good porosity, which could bring better bone-implant integration than solid screw [44–46]. Therefore, auxetic structures could be a prospective direction of bone screws. However, biomechanical investigations on the structure design are still lack. A study is necessary to demonstrate the mechanical merit of auxetic bone screws possessing auxetic behavior.

In this study, six kinds of auxetic unit cells were designed and evaluated, and then introduced to the design of bone screw body. Tensile tests on the designed tubular structures composed of the above units were conducted experimentally and computationally. It was found that re-entrant structures (A1, A2) had higher tensile stiffness and strength due to the von Mises stress distribution of these structural types was more uniform under tensile loading. Rotating structures (A5, A6) had better auxetic behavior due to the instability under tensile loading would easy to cause large deformation (Fig. 9). Besides, the result that TA4 composed of had smaller auxetic deformation was in line with those of Ren et al. [16]. These findings suggested that the mechanical properties of the auxetic structures could be partially predictable upon their structural types. This would provide supportive evidence to selecting suitable auxetic structure base on specific application purposes. The mechanical properties of tubular structures with varied thicknesses were evaluated. It was found that tensile stiffness & strength and breaking elongation increased as the wall thickened (from 0.8 to 1.2 mm), while the Poisson's ratios were almost not changed. To improve stiffness and strength of tubular auxetic structure without affecting its auxetic deformation, wall thickness could be increased appropriately.

Six auxetic bone screws were designed and fabricated, then tensile mechanical properties and pullout fixation strength were evaluated. Auxetic deformation was observed among all designed auxetic screws in the tensile test experimentally and computationally. A good combination of stiffness, strength, and auxetic behavior was found predictably in AS2. Super auxetic performance was found in AS5, while poor stiffness and strength were also found. These indicated that the auxetic behavior of bone screw could be obtained by introducing auxetic unit cell into screw body, and type of unit cell is the most important factor that

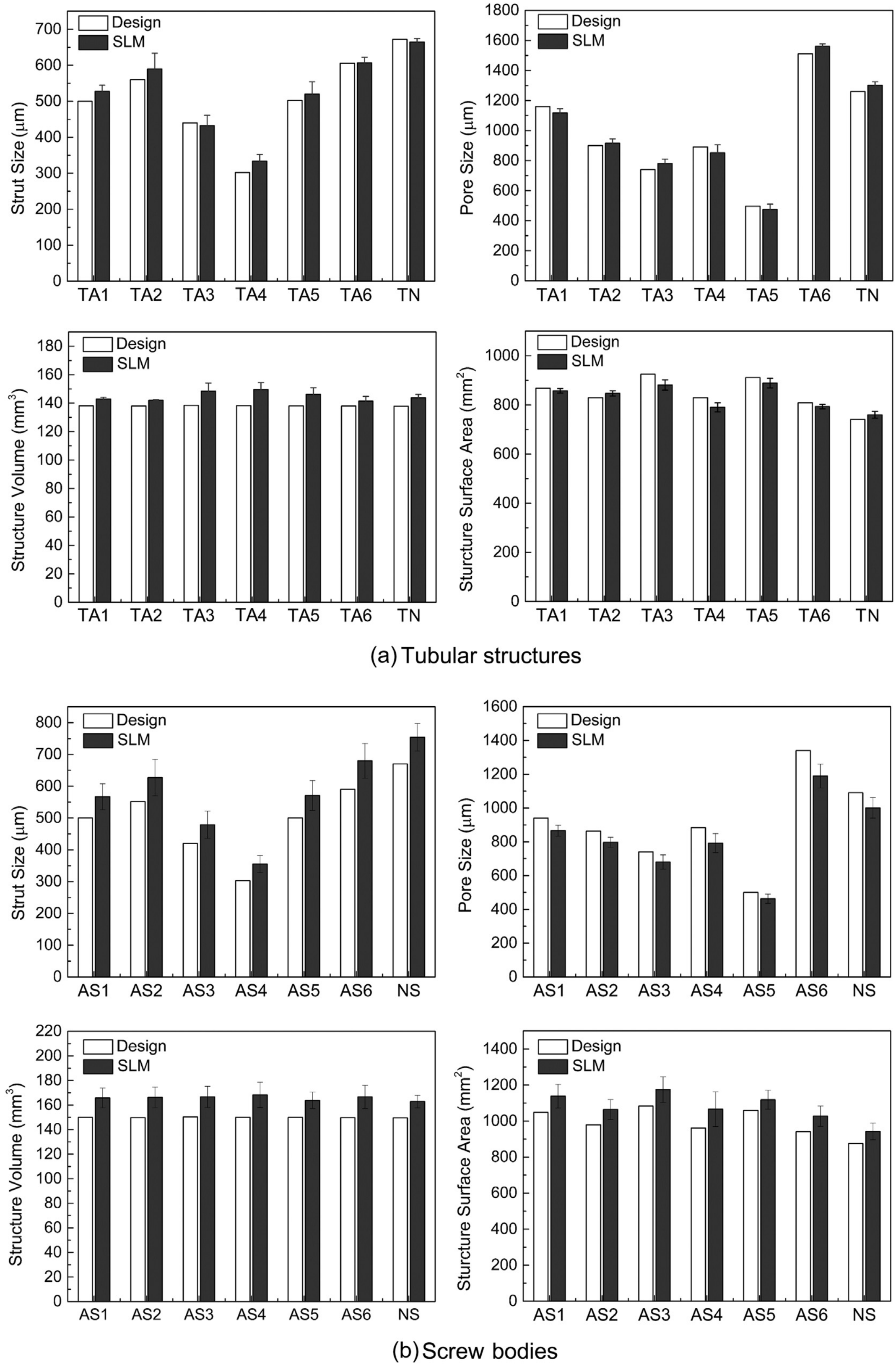

Fig. 5. Details of SLM manufactured structures with different unit cells in comparison to original designs: (a) fabricated tubular structures; (b) fabricated screw bodies.

affected the auxetic performance of designed screw. Besides, although prediction and assessment by FEA results were consistent with EXP results, but it also indicated discrepancy between FEA and EXP for the specimens of screws: stiffness, strength and Poisson's ratio calculated by FEA is higher than EXP values. Actually, studies of Li et al. [47], Pei et al. [48] and other researchers [49] also had found this phenomenon. In this study, morphologies characterization of specimens might provide some reasons for the abovementioned phenomenon. The original

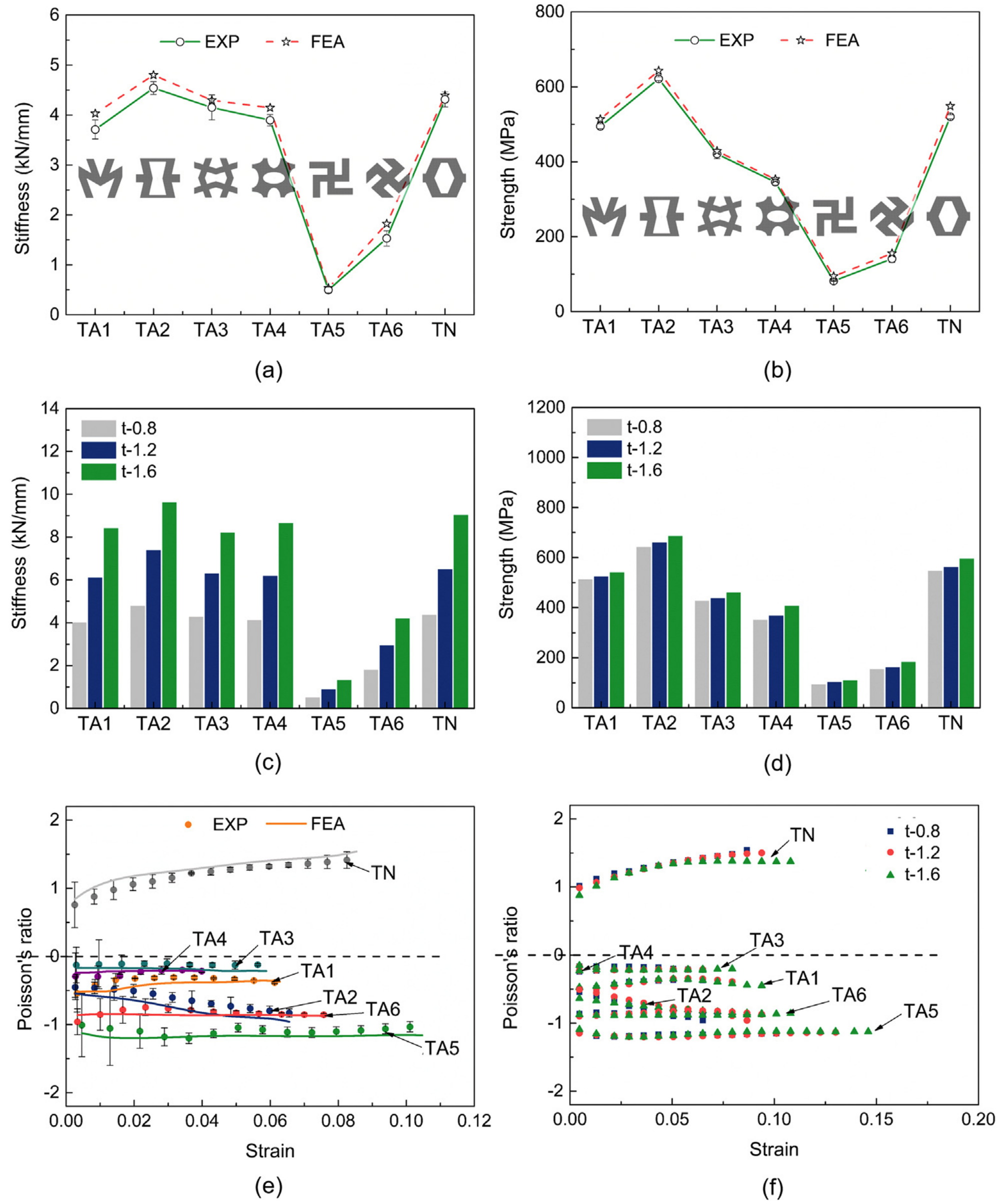

Fig. 6. Mechanical properties of the designed tubular structures: (a), (b) Tensile stiffness and strength (t = 0.8 mm) obtained both by EXP and FEA; (c), (d) Tensile stiffness and strength (t = 0.8, t = 1.2, t = 1.6 mm) obtained by FEA; (e) Poisson's ratio (t = 0.8 mm) obtained both by EXP and FEA; (f) Poisson's ratio (t = 0.8, t = 1.2, t = 1.6 mm) obtained by FEA.

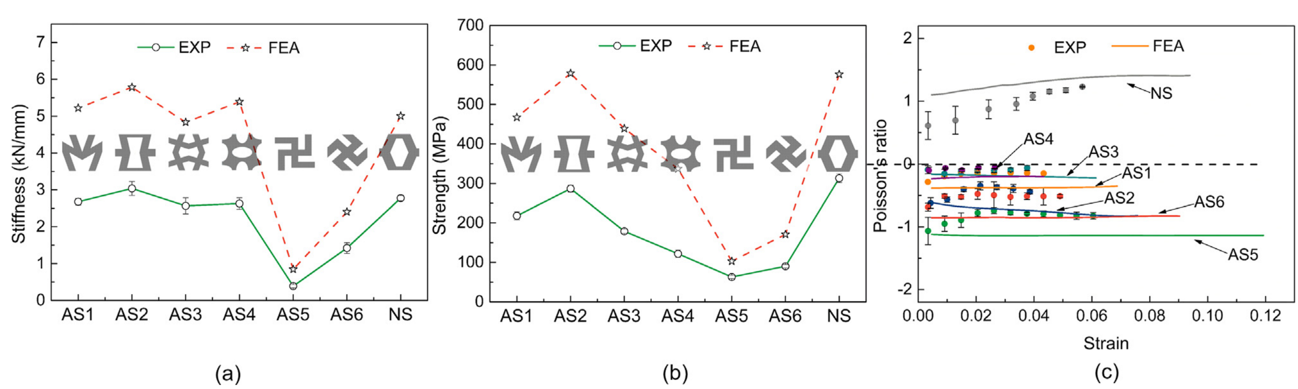

Fig. 7. Mechanical properties of bone screws (t = 1.6 mm): (a) Tensile stiffness obtained both by EXP and FEA; (b) Tensile strength obtained both by EXP and FEA; (c) Poisson's ratio obtained both by EXP and FEA.

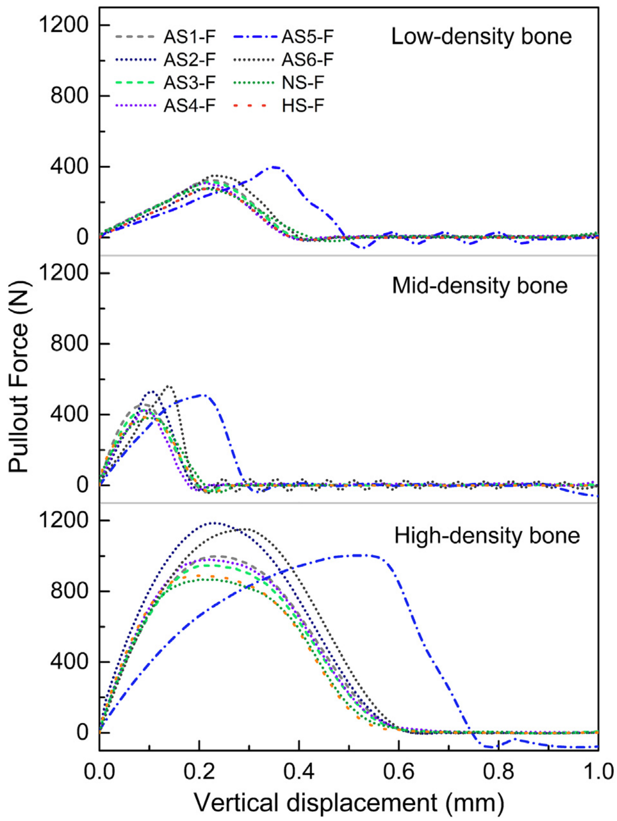

Fig. 8. Pulling forces of bone screws: Pullout performances in Low-density bone, Mid-density bone, and High-density bone.

designed screws were not well reproduced by 3D printer, some mismatches in the macro and micro morphologies were found. Thread of designed screws with a lot of small geometric features, which were not accurately manufactured due to limitations of metal 3D printing technology. This mismatch would inevitably affect the mechanical properties of screw. Therefore, the accuracy manufacture is necessary to assure the mechanical properties of the designed screws.

The fixation strength of designed bone screws was evaluated by simulating the bone-pullout process computationally. It was found that auxetic deformation of the auxetic bone screw would increase the bone-screw fixation. But the auxetic deformation was depended on not only the NPR and stiffness of screw, but also the density of surrounding bone. To explain this phenomenon, the behaviors of bone and designed screws during the pullout process were analyzed in detail. AS2 and AS5 in three kinds of bones were taken as an example. The von Mises stress and shear stress contours of the bone at the peak load were showed in Fig. 10a and b respectively. It was seen that the bone experienced significant shear stress around the thread during screw pullout. The stress distributed of bone almost equally among the threads of AS2 (compared with AS5), which finally failed at the same time before the screw was completed pulled out. AS5 with the lowest stiffness was easily elongated under tensile load, which caused high stress concentrated at the thread root. Those stress concentration regions reached the yield point and failed (locations firstly failed were shown in the red dotted box), which would reduce the anti-pullout property of screw. This might be the reason why AS5 had better auxetic performance than AS2 but lower pullout force than that of AS2 in bones with mid- and high-density. The radial displacement of AS2 and AS5 increased with the increasing of bone density, showing better and better auxetic performance (Fig. 10c). It was indicated that high-bone-density could provide good anchor to distal screw, which might be a prerequisite for showing auxetic performance of auxetic bone screw. While increasing of bone density might inhibit the auxetic deformation by preventing the screw from expanding. To assure the auxetic deformation of auxetic screw, novel designs were needed to improve the distal fixation for various bone-density conditions. Besides, how does the strength, stiffness and surrounding bone density affect the auxetic deformation of the auxetic bone screw under pullout load should be further studied urgently.

Finally, there are still some limitations in this study. The bone-pullout processes were conducted only by computational simulation. The pullout force might differ from the actual force values, but this did not affect the comparison of forces between different screws. It is

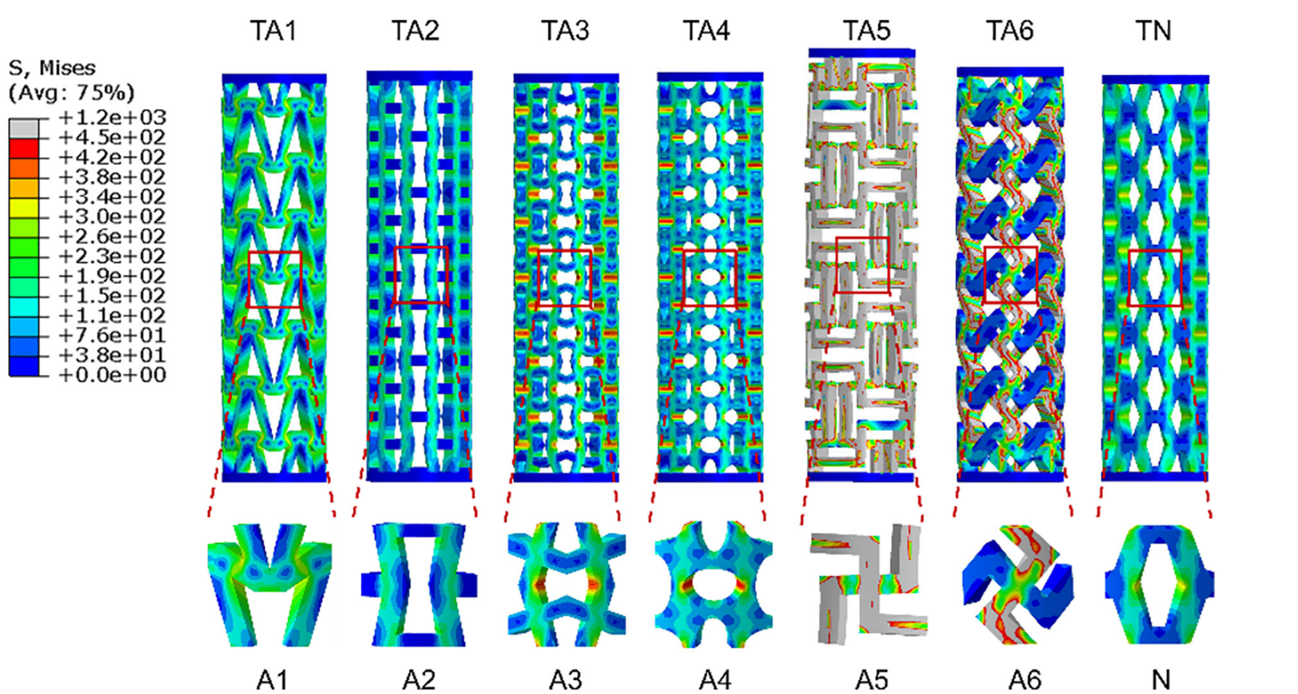

Fig. 9. Von Mises stress distribution of tubular structures (t = 0.8 mm) under tensile loading (600 N): Tubular structures (TA1–TA6, and TN); Unit cells (A1–A6, and N) of tubular structure (unit cell locations were shown in the red box).

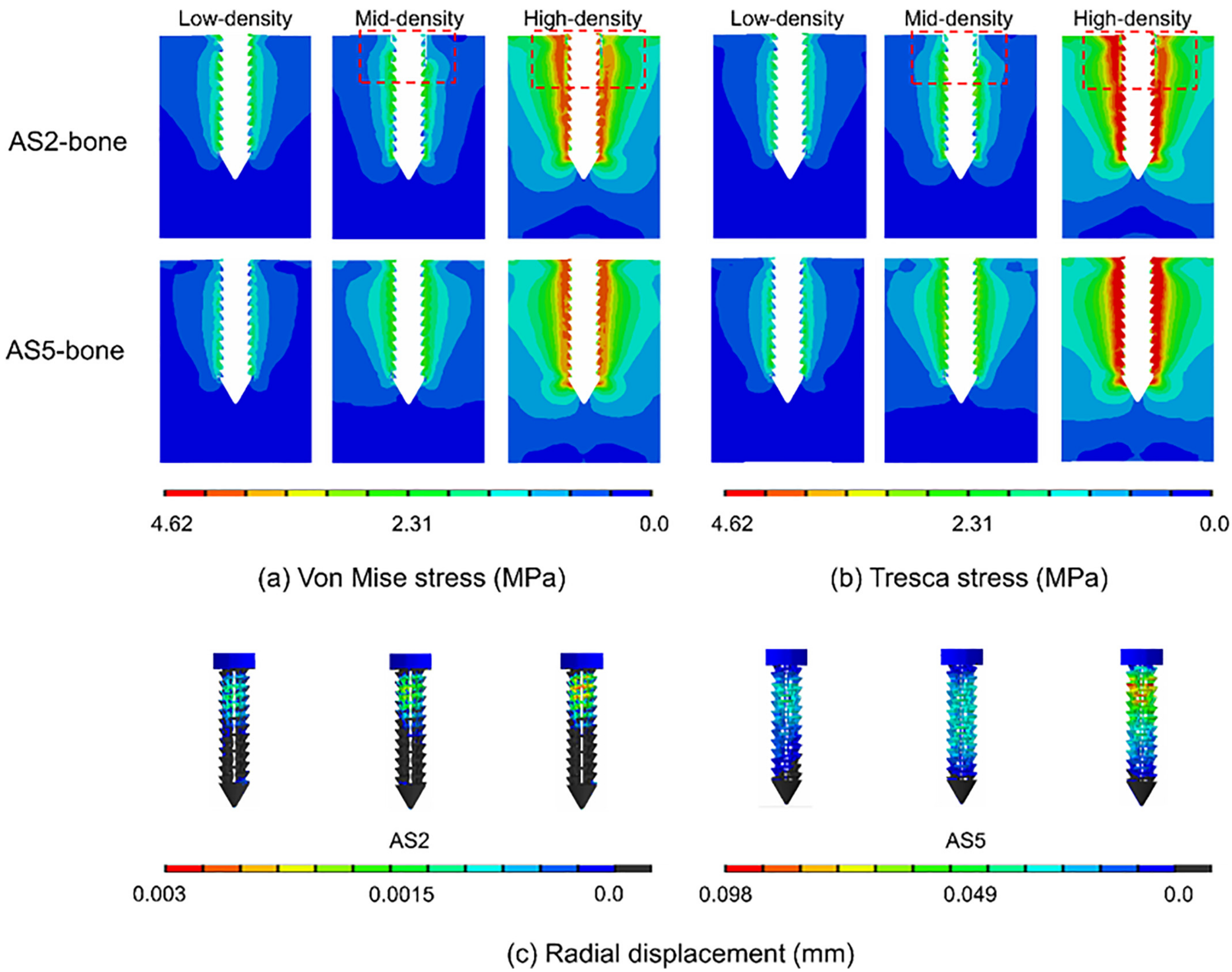

Fig. 10. The anti-pullout performances of AS2 and AS5 in three kinds of bones (at the peak pullout force): (a) Vertical-sectional views through the bone showing the von Mise stress distribution; (b) Vertical-sectional views through the bone showing the tresca stress distribution; (c) Radial displacement distributions of AS2 and AS5.

difficult to control the additional factors that influence the pull-out force in the pullout test on real auxetic screw. More suitable test method was needed to design in the future research. In addition, the evaluations of torsion of bone screw were not conducted in this study. Auxetic bone screw would shrink under contraction caused by the NPR property, which would lead to unprecedented interactions between bone and screw. To explore this interesting and meaning possible phenomenon, a series of tests and simulations would be conducted carefully in following research. Besides, the designed auxetic bone screw could present well performance in stiffness & strength, but still less than solid and hollow bone screw used in clinic. The stiffness and strength of auxetic bone screw would be improved by the in-growth of bone tissue. Therefore, the evaluation to the strength and stiffness of auxetic bone screws during the osseointegration is necessary in future studies. Finally, due to limitations of 3D printing technology, the fabricated auxetic bone screws showed lower stiffness, strength and auxetic deformation than that calculated used by verified FE models. The study of the accuracy fabrication of the auxetic bone screws is urgent to promote the clinical application. The fabrication accuracy of auxetic bone screw might be improved by 1) optimizing unit cell shape (such as smoothing the sharp corners) and SLM printing parameters (including scanning speed and path); 2) exploring different materials, such as biocompatible photosensitive resin that available for the nanoscale 3D printers (resolution of ~10 μm).

6. Conclusion

In this study, the novel design of auxetic bone screws were proposed to help improve the bone-screw fixation. The feasibility of auxetic bone screws was explored by evaluating the tensile performance and fixation strength of screws composed of different auxetic structures. The following conclusions could be drawn:

(1) Auxetic bone screws can be obtained by introducing auxetic unit cells to the design of screw body.
(2) The designed screws could be fabricated by SLM rapid prototyping process. The molten layers of printed screws were metallurgical bonding without interlayer delamination.
(3) Changes of auxetic structure type altered screw's mechanical properties especially its functional properties. Auxetic bone screw composed of re-entrant structures (A1, A2) and chiral structures (A3, A4) had better tensile stiffness and strength, and that composed of re-entrant structures (A1, A2) and rotating structures (A5, A6) had better auxetic performance.
(4) The bone-screw fixation could be improved by auxetic structures while it is also affected by other design factors (including screw strength and stiffness, the density of surrounding bone). In the high-density bone, AS2 owning better NPR and the best stiffness had the best anti-pullout performance. In the low-density bone,

AS5 owning the best NPR and smallest stiffness had the best anti-pullout performance.

CRediT authorship contribution statement

Yan Yao: Investigation, Writing - original draft. **Lizhen Wang:** Conceptualization, Writing - review & editing. **Jian Li:** Software. **Shan Tian:** Validation. **Ming Zhang:** Resources. **Yubo Fan:** Supervision.

Declaration of competing interest

The authors declare that they have no known competing financial interests or personal relationships that could have appeared to influence the work reported in this paper.

Acknowledgement

This work was funded by grants from the National Natural Science Foundation of China (No. 11421202, No. 11822201, No. 11572029) and supported by China National Key Research and Development Plan Project (NO. 2016YFB1101100).

Appendix A. Supplementary data

Supplementary data to this article can be found online at https://doi.org/10.1016/j.matdes.2019.108424.

References

[1] P.F. Stahel, N.A. Alfonso, C. Henderson, T. Baldini, Introducing the "Bone-Screw-Fastener" for improved screw fixation in orthopedic surgery: a revolutionary paradigm shift? Patient Saf Surg. 11 (2017) 1–8, https://doi.org/10.1186/s13037-017-0121-5.

[2] R. Vaishya, M. Chauhan, A. Vaish, Bone cement, J. Clin. Orthop. Trauma. 4 (2013) 157–163, https://doi.org/10.1016/j.jcot.2013.11.005.

[3] S.W. Kim, H. Shin, J.K. Kim, C. Il Ju, J.H. Seo, Clinical efficacy of bone cement augmented screw fixation for the severe osteoporotic spine, Korean J. Spine. 9 (2015) 79–84, https://doi.org/10.14245/kjs.2012.9.2.79.

[4] Y.Y. Kim, W.S. Choi, K.W. Rhyu, Assessment of pedicle screw pullout strength based on various screw designs and bone densities - an ex vivo biomechanical study, Spine J. 12 (2012) 164–168, https://doi.org/10.1016/j.spinee.2012.01.014.

[5] T. Wang, C. Boone, A.W. Behn, J.B. Ledesma, J.A. Bishop, Cancellous screws are biomechanically superior to cortical screws in metaphyseal bone, Orthopedics 39 (2016) e828–e832, https://doi.org/10.3928/01477447-20160509-01.

[6] R.J. Van Arkel, S. Ghouse, P.E. Milner, J.R.T. Jeffers, Additive manufactured push-Fit implant fixation with screw-strength pull out, J. Orthop. Res. 36 (2018) 1508–1518, https://doi.org/10.1002/jor.23771.

[7] J.B. Choi, R.S. Lakes, Non-linear properties of polymer cellular materials with a negative Poisson's ratio, J. Mater. Sci. 27 (1992) 4678–4684, https://doi.org/10.1007/BF02403846.

[8] Y. Ma, F. Scarpa, D. Zhang, B. Zhu, L. Chen, J. Hong, A nonlinear auxetic structural vibration damper with metal rubber particles, Smart Mater. Struct. 22 (2013) 1–9, https://doi.org/10.1088/0964-1726/22/8/084012.

[9] Y. Li, S. Luo, M.C. Yang, R. Liang, C. Zeng, Poisson ratio and piezoresistive sensing: a new route to high-performance 3D flexible and stretchable sensors of multimodal sensing capability, Adv. Funct. Mater. 26 (2016) 2900–2908, https://doi.org/10.1002/adfm.201505070.

[10] S.K. Bhullar, D. Rana, H. Lekesiz, A.C. Bedeloglu, J. Ko, Y. Cho, Z. Aytac, T. Uyar, M. Jun, M. Ramalingam, Design and fabrication of auxetic PCL nanofiber membranes for biomedical applications, Mater. Sci. Eng. C. 81 (2017) 334–340, https://doi.org/10.1016/j.msec.2017.08.022.

[11] Y. Yan, Y. Li, L. Song, C. Zeng, Y. Li, Pluripotent stem cell expansion and neural differentiation in 3-D scaffolds of tunable Poisson's ratio, Acta Biomater. 49 (2017) 192–203, https://doi.org/10.1016/j.actbio.2016.11.025.

[12] E.N. Feins, Y. Lee, E.D. O'Cearbhaill, N.V. Vasilyev, S. Shimada, I. Friehs, D. Perrin, P.E. Hammer, H. Yamauchi, G. Marx, A. Gosline, V. Arabagi, J.M. Karp, P.J. Del Nido, A growth-accommodating implant for paediatric applications, Nat. Biomed. Eng. 1 (2017) 818–825, https://doi.org/10.1038/s41551-017-0142-5.

[13] J.N. Grima, R. Caruana-Gauci, M.R. Dudek, K.W. Wojciechowski, R. Gatt, Smart metamaterials with tunable auxetic and other properties, Smart Mater. Struct. 22 (2013) 1–11, https://doi.org/10.1088/0964-1726/22/8/084016.

[14] J.N. Grima, A. Alderson, K.E. Evans, Auxetic behaviour from rotating rigid units, Mater. Res. 575 (2005) 561–575, https://doi.org/10.1002/pssb.200460376.

[15] J.N. Grima, P.S. Farrugia, R. Gatt, D. Attard, On the auxetic properties of rotating rhombi and parallelograms: a preliminary investigation, Phys. Status Solidi Basic Res. 245 (2008) 521–529, https://doi.org/10.1002/pssb.200777705.

[16] X. Ren, J. Shen, P. Tran, T.D. Ngo, Y.M. Xie, Auxetic nail: design and experimental study, Compos. Struct. 184 (2018) 288–298, https://doi.org/10.1016/j.compstruct.2017.10.013.

[17] M.H. Fu, Y. Chen, L.L. Hu, A novel auxetic honeycomb with enhanced in-plane stiffness and buckling strength, Compos. Struct. 160 (2017) 574–585, https://doi.org/10.1016/j.compstruct.2016.10.090.

[18] Z.X. Lu, X. Li, Z.Y. Yang, F. Xie, Novel structure with negative Poisson's ratio and enhanced Young's modulus, Compos. Struct. 138 (2016) 243–252, https://doi.org/10.1016/j.compstruct.2015.11.036.

[19] K. Doi, T. Kubo, S. Kajihara, Y. Makihara, H. Oue, Y. Oki, V. Perrotti, A. Piattelli, Y. Akagawa, K. Tsuga, A stability evaluation of a novel titanium dental implant/interconnected porous hydroxyapatite complex under functional loading conditions, Dent. Mater. J. 36 (2017) 647–653, https://doi.org/10.4012/dmj.2016-346.

[20] J.W. Lee, H.B. Wen, P. Gubbi, G.E. Romanos, New bone formation and trabecular bone microarchitecture of highly porous tantalum compared to titanium implant threads: a pilot canine study, Clin. Oral Implants Res. 29 (2018) 164–174, https://doi.org/10.1111/clr.13074.

[21] R. Mozafar Shokri, P. Yunan, A. Zaini, Analytical solution and finite element approach to the 3D re-entrant structures of auxetic materials, Mech. Mater. 74 (2014) 76–87, https://doi.org/10.1016/j.mechmat.2014.03.012.

[22] D. Rayneau-Kirkhope, C. Zhang, L. Theran, M.A. Dias, Analytic analysis of auxetic metamaterials through analogy with rigid link systems, Proc. R. Soc. A Math. Phys. Eng. Sci. 474 (2018) https://doi.org/10.1098/rspa.2017.0753.

[23] L. Valentini, S. Bittolo Bon, N.M. Pugno, Graphene and carbon nanotube auxetic rubber bionic composites with negative variation of the electrical resistance and comparison with their nonbionic counterparts, Adv. Funct. Mater. 27 (2017) 1–19, https://doi.org/10.1002/adfm.201606526.

[24] P. Vogiatzis, S. Chen, X. Wang, T. Li, L. Wang, Topology optimization of multi-material negative Poisson's ratio metamaterials using a reconciled level set method, CAD Comput. Aided Des. 83 (2017) 15–32, https://doi.org/10.1016/j.cad.2016.09.009.

[25] J. Zeng, H. Hu, L. Zhou, A study on negative Poisson's ratio effect of 3D auxetic orthogonal textile composites under compression, Smart Mater. Struct. 26 (2017) 1–15, https://doi.org/10.1088/1361-665X/aa6fe6.

[26] H. Zhang, Y. Luo, Z. Kang, Bi-material microstructural design of chiral auxetic metamaterials using topology optimization, Compos. Struct. 195 (2018) 232–248, https://doi.org/10.1016/j.compstruct.2018.04.058.

[27] T.C. Lim, Analogies across auxetic models based on deformation mechanism, Phys. Status Solidi - Rapid Res. Lett. 11 (2017) 1–14, https://doi.org/10.1002/pssr.201600440.

[28] N.D. Duc, K. Seung-Eock, N.D. Tuan, P. Tran, N.D. Khoa, New approach to study nonlinear dynamic response and vibration of sandwich composite cylindrical panels with auxetic honeycomb core layer, Aerosp. Sci. Technol. 70 (2017) 396–404, https://doi.org/10.1016/j.ast.2017.08.023.

[29] T. Li, Y. Chen, X. Hu, Y. Li, L. Wang, Exploiting negative Poisson's ratio to design 3D-printed composites with enhanced mechanical properties, Mater. Des. 142 (2018) 247–258, https://doi.org/10.1016/j.matdes.2018.01.034.

[30] X. Ren, J. Shen, P. Tran, T.D. Ngo, Y.M. Xie, Design and characterisation of a tuneable 3D buckling-induced auxetic metamaterial, Mater. Des. 139 (2018) 336–342, https://doi.org/10.1016/j.matdes.2017.11.025.

[31] S. Yuan, F. Shen, J. Bai, C.K. Chua, J. Wei, K. Zhou, 3D soft auxetic lattice structures fabricated by selective laser sintering: TPU powder evaluation and process optimization, Mater. Des. 120 (2017) 317–327, https://doi.org/10.1016/j.matdes.2017.01.098.

[32] X. Hou, V.V. Silberschmidt, Metamaterials with Negative Poisson's Ratio: a review of mechanical properties and deformation mechnaisms, Mech. Adv. Mater. (2015) 155–179, https://doi.org/10.1007/978-3-319-17118-0_7Springer International Publishing.

[33] I. Bružauskaitė, D. Bironaitė, E. Bagdonas, E. Bernotienė, Scaffolds and cells for tissue regeneration: different scaffold pore sizes-different cell effects, Cytotechnology 68 (2016) 355–369, https://doi.org/10.1007/s10616-015-9895-4.

[34] N. Taniguchi, S. Fujibayashi, M. Takemoto, K. Sasaki, B. Otsuki, T. Nakamura, T. Matsushita, T. Kokubo, S. Matsuda, Effect of pore size on bone ingrowth into porous titanium implants fabricated by additive manufacturing: an in vivo experiment, Mater. Sci. Eng. C. 59 (2016) 690–701, https://doi.org/10.1016/j.msec.2015.10.069.

[35] Z. Wang, C. Wang, C. Li, Y. Qin, L. Zhong, B. Chen, Z. Li, H. Liu, F. Chang, J. Wang, Analysis of factors influencing bone ingrowth into three-dimensional printed porous metal scaffolds: a review, J. Alloys Compd. 717 (2017) 271–285, https://doi.org/10.1016/j.jallcom.2017.05.079.

[36] P. Newman, H. Zreiqat, Design and fabrication of 3D printed scaffolds with a mechanical strength comparable to cortical bone to repair large bone defects, Nat. Publ. Gr. 19468 (2016) 1–8, https://doi.org/10.1038/srep19468.

[37] T. Schouman, M. Schmitt, C. Adam, G. Dubois, P. Rouch, Influence of the overall stiffness of a load-bearing porous titanium implant on bone ingrowth in critical-size mandibular bone defects in sheep, J Mech Behav Biomed. 76 (2017) (2017) 1328–1343, https://doi.org/10.1016/j.msec.2017.02.094.

[38] X.P. Tan, Y.J. Tan, C.S.L. Chow, S.B. Tor, W.Y. Yeong, Metallic powder-bed based 3D printing of cellular scaffolds for orthopaedic implants: a state-of-the-art review on manufacturing, topological design, mechanical properties and biocompatibility, Mater. Sci. Eng. C. 76 (2017) 1328–1343, https://doi.org/10.1016/j.msec.2017.02.094.

[39] A. Dorogoy, D. Rittel, K. Shemtov-Yona, R. Korabi, Modeling dental implant insertion, J. Mech. Behav. Biomed. Mater. 68 (2017) 42–50, https://doi.org/10.1016/j.jmbbm.2017.01.021.

[40] H. Guan, R.C. Van Staden, N.W. Johnson, Y.C. Loo, Dynamic modelling and simulation of dental implant insertion process-a finite element study, Finite Elem. Anal. Des. 47 (2011) 986–997, https://doi.org/10.1016/j.finel.2011.03.005.

[41] R. Bianco, P. Arnoux, E. Wagnac, C. Aubin, Minimizing pedicle screw pullout risks: a detailed biomechanical analysis of screw design and placement, Clin Spine Surg 30 (2017) 226–232, https://doi.org/10.1097/BSD.0000000000000151.

[42] D.L. Kopperdahl, T.M. Keaveny, Yield strain behavior of trabecular bone, J. Biomech. 31 (1998) 601–608, https://doi.org/10.1016/s0021-9290(98)00057-8.
[43] B. Li, R.M. Aspden, Composition and mechanical properties of cancellous bone from the femoral head of patients with osteoporosis or osteoarthritis, J. Bone Miner. Res. 12 (1997) 641–651, https://doi.org/10.1359/jbmr.1997.12.4.641.
[44] F. Yang, C. Chen, Q. Zhou, Y. Gong, R. Li, C. Li, F. Klämpfl, S. Freund, X. Wu, Y. Sun, X. Li, M. Schmidt, D. Ma, Y. Yu, Laser beam melting 3D printing of Ti6Al4V based porous structured dental implants: fabrication, biocompatibility analysis and photoelastic study, Sci. Rep. 7 (2017) 1–12, https://doi.org/10.1038/srep45360.
[45] D.G. Kim, Y.H. Jeong, H.H. Chien, A.M. Agnew, J.W. Lee, H.B. Wen, Immediate mechanical stability of threaded and porous implant systems, Clin. Biomech. 48 (2017) 110–117, https://doi.org/10.1016/j.clinbiomech.2017.08.001.
[46] P.I. Tsai, C.Y. Chen, S.W. Huang, K.Y. Yang, T.H. Lin, S.Y. Chen, J.S. Sun, Improvement of bone-tendon fixation by porous titanium interference screw: a rabbit animal model, J. Orthop. Res. 36 (2018) 2633–2640, https://doi.org/10.1002/jor.24037.
[47] J. Li, D. Chen, Y. Zhang, Y. Yao, Z. Mo, Diagonal-symmetrical and midline-symmetrical unit cells with same porosity for bone implant: mechanical properties evaluation, J Bionic Eng 16 (2019) 468–479, https://doi.org/10.1007/s42235-019-0038-z.
[48] X. Pei, B. Zhang, Y. Fan, X. Zhu, Y. Sun, Q. Wang, X. Zhang, Bionic mechanical design of titanium bone tissue implants and 3D printing manufacture, Mater. Lett. 208 (2017) 133–137, https://doi.org/10.1016/j.matlet.2017.04.128.
[49] L. Wang, J. Kang, C. Sun, D. Li, Y. Cao, Z. Jin, Mapping porous microstructures to yield desired mechanical properties for application in 3D printed bone scaffolds and orthopaedic implants, Mater. Des. 133 (2017) 62–68, https://doi.org/10.1016/j.matdes.2017.07.021.